Journal of Solid State Chemistry **155,** 55–61 (2000)
doi:10.1006/jssc.2000.8891, available online at http://www.idealibrary.com on IDEAL®

$Yb_5In_2Sb_6$: A New Rare Earth Zintl Phase with a Narrow Band Gap

Sung-Jin Kim,*,[1] John R. Ireland,† Carl R. Kannewurf,† and Mercouri G. Kanatzidis*,[2]

*Department of Chemistry and Center for Fundamental Materials Research, Michigan State University, East Lansing, Michigan 48824; and
†Department of Electrical Engineering and Computer Science, Northwestern University, Evanston, Illinois, 60208.

Received May 30, 2000; in revised form July 18, 2000; accepted July 27, 2000

DEDICATED TO PROFESSOR J. M. HONIG

The new Zintl phase $Yb_5In_2Sb_6$ was obtained from a direct element combination reaction in a sealed graphite tube at 700°C and its structure was determined. It crystallizes in the orthorhombic space group *Pbam* (No. 55), in the $Ba_5Al_2Bi_6$ structure type, with a unit cell of $a=7.3992(5)$ Å, $b=23.001(6)$ Å, $c=4.5139(4)$ Å, and $Z=2$. $Yb_5In_2Sb_6$ has a one-dimensional structure with infinite anionic double chains $(In_2Sb_6)^{10-}$ separated by Yb^{2+} ions. Each single chain is made of corner-sharing $InSb_4$ tetrahedra. Two such chains are bridged by Sb_2 groups to form double chains $\frac{1}{\infty}[In_2Sb_6^{10-}]$. The compound satisfies the classical Zintl concept and is a narrow gap semiconductor. Band structure calculations suggest an direct band gap. Polycrystalline ingots of $Yb_5In_2Sb_6$ showed electrical conductivity of 100 S/cm and a Seebeck coefficient of $\sim +30$ μV/K at room temperature. The thermal conductivity of $Yb_5In_2Sb_6$ is about 1.7 W/mK in the temperature range of 150–300 K. © 2000 Academic Press

INTRODUCTION

Currently there is substantial interest for improved thermoelectric materials (1, 2). Zintl phases represent a potential class from which to draw new thermoelectric materials because of many attractive structural and bonding characteristics found in many of its members (3, 4). Namely, their complex anionic frameworks, stabilized by weakly bounded positive cations, are reminiscent of those found in many bismuth chalcogenide compounds (5). Unfortunately, the great majority of Zintl phases are reported to be air- and moisture-sensitive, primarily because of the highly electropositive elements, such as alkali and alkaline earth metals. For example, in a given system, T1 analogues are more stable than K analogues and Yb or Eu analogues tend to be more stable than Sr and Ba analogues (6). For thermoelectric applications, air- and moisture-stable compounds are necessary, and this may be achieved with the use of heavier, softer electropositive elements. Furthermore, heavy element analogues of the Zintl phases are expected to be narrow-gap semiconductors, which is important for thermoelectric properties.

Recently, we have synthesized the new air-stable Zintl phases, $Ba_4In_8Sb_{16}$ (3a) $BaGa_2Sb_2$ (3b), and Ba_6Ge_{24} (3c). In an extension of this work, we turned to Zintl phases with rare earth cations. In some intermetallic materials, the *f* electrons of rare earth elements such as Ce, Sm, Eu, Tm, and Yb are known to be responsible for unusual electronic transport properties, especially, high thermopower (7). These elements might cause favorable modifications in the band structure of semiconducting Zintl phases around the Fermi level (by way of mixed valency, for example).

Here we describe the new compound $Yb_5In_2Sb_6$, which is the first rare earth analogue of the $A_5M_2Pn_6$ (A = Ca, Sr, Ba; M = Ga, Al; Pn = In, Bi) family. We report the synthesis, crystal structure, spectroscopic properties, and electronic structure of this compound. A preliminary assessment of its thermoelectric properties including electrical conductivity, thermopower, and thermal conductivity are also reported.

EXPERIMENTAL SECTION

Synthesis. A reaction mixture composed of Yb (0.865 g, 5 mmol), In (0.229, 2 mmol), and Sb (0.730 g 6 mmol), was placed in a graphite tube and then sealed in an evacuated silica tube. The mixture was heated slowly (over 4 days) up to 700°C, kept at that temperature for 1 day, and subsequently cooled to room temperature over 1 day. A few bar-shaped black crystals were obtained, along with gray featureless pieces. Semiquantitative microprobe analysis on several single crystals gave "$Yb_{5.0}In_{1.8}Sb_{7.1}$." The X-ray powder diffraction pattern of the bulk sample agreed well with the powder pattern calculated from single-crystal data indicating that the gray featureless pieces were $Yb_5In_2Sb_6$.

[1] Permanent address: Department of Chemistry, Ewha Women's University, Seoul, Korea, 120–750.
[2] To whom correspondence should be addressed. E-mail: Kanatzid@cem.msu.edu.

0022-4596/00 $35.00

Electron microscopy. Semiquantitative microprobe analysis of the compounds was performed with a JEOL JSM-35C scanning electron microscope (SEM) equipped with a Tracor Northern Energy Dispersive Spectroscopy (EDS) detector. Data were acquired using an accelerating voltage of 20 kV and a 30-s accumulation time. The results reported are an average of multiple measurements done on several single crystals.

Charge-transport measurements. DC electrical conductivity and thermopower measurements were made on a polycrystalline pellet with dimensions of $2 \times 2 \times 5$ mm. The pellet was sintered in an evacuated graphite container at 500°C for 2 h. Conductivity measurement was performed in the usual four-probe geometry with 60- and 25-m gold wires used for the current and voltage electrodes, respectively. Measurements of the sample cross-sectional area and voltage probe separation were made with a calibrated binocular microscope. The data were obtained with the computer-automated system described elsewhere (8a). Thermoelectric power measurements were made by using a slow AC technique (8b) with 60-m gold wires serving to support and conduct heat to the sample, as well as to measure the voltage across the sample resulting from the applied temperature gradient. In both measurements, the gold electrodes were held in place on the sample with a conductive gold paste.

Differential thermal analysis. Differential thermal analysis (DTA) was performed with a Shimadzu DTA-50 thermal analyzer. The ground sample (~ 20.0 mg total mass) was sealed in a carbon-coated silica ampule under vacuum. A silica ampule containing alumina of equal mass was sealed and placed on the reference side of the detector. The sample was heated to 800°C at 10°C/min and isothermed for 10 min, followed by cooling at -10°/min to 50°C. The stability and reproducibility of the sample was monitored by running multiple heating/cooling cycles. The residue of the DTA experiment was examined with X-ray powder diffraction.

Electronic structure calculations. Electronic structure calculations were performed using the Hückel method within the framework of the tight-binding approximation (9). The program CAESAR for IBM-compatible PCs was used (10). Density of states (DOS) and crystal orbital overlap populations (COOP) were calculated based on 216 K point sets of the primitive orthorhombic structure.

Crystallographic studies. A black bar-shaped crystal with $0.03 \times 0.02 \times 0.06$ mm was mounted on a glass fiber. A Siemens SMART Platform CCD diffractometer was used to collect intensity data using graphite monochromatized Mo$K\alpha$ radiation. The data were collected over a full sphere of reciprocal space up to 56° in 2θ. The individual frames were measured with an ω rotation of 0.3° and an acquisition time of 30 s. To check the stability of the crystal, at the end of the data collection procedure the initial 50 frames of data were measured again and compared. No crystal decay was detected. The SMART software (11) was used for data acquisition and SAINT (12) for data extraction and reduction. The absorption correction was performed empirically using SADABS (12). The unit cell parameters were obtained from least-squares refinement using randomly chosen 600 reflections from a full sphere of reciprocal space up top 56° in 2θ. The observed Laue symmetry and systematic extinctions were indicative of the space groups *Pbam* or *Pba2*. The centrosymmetric *Pbam* was assumed, and subsequent refinements confirmed the choice of this space group. The initial positions of all atoms were obtained from direct methods. The structure was refined by full-matrix least-squares techniques with the SHELXTL (13) package of crystallographic program. Once all atoms were located, the occupancies of successive atoms were allowed to vary, but refinements did not lead to any significant change in the occupation factor. The final cycle of refinement performed on F_o^2 with 42 variables and 1029 averaged reflections converged to residuals wR_2 $(F_o^2 > 0) = 0.0746$. On the other hand, the conventional R index based on reflections having $F_o^2 > 2\sigma(F_o^2)$ was 0.0274. A difference electron density Fourier map calculated with phases based on the final parameters showed maximum and minimum peaks of 1.981 and -1.974 e/Å^3, respectively. The complete data collection parameters and details of structure solution and refinement results are given in Table 1. Final atomic positions, displacements parameters, and anisotropic displacement parameters are given in Tables 2 and 3. Selected bond distances and angles are listed in Table 4.

TABLE 1
Selected Data from the Single-Crystal Structure Refinement of $Yb_5In_2Sb_6$

Empirical formula	$Yb_5In_2Sb_6$
Formula weight	3650.68
Temperature (K)	293(2)
Wavelength ($\lambda = K\alpha$, Å)	0.71073
Crystal system	Orthorhombic
Space group	*Pbam* (No. 55)
Unit cell dimensions (Å)	$a = 7.3992(5)$
	$b = 23.001(6)$
	$c = 4.5139(4)$
Volume (Å^3)	768.2(3)
Z	2
Density, ρ_{calc} (g/cm^3)	7.891
Absorption coefficient (mm^{-1})	43.342
Reflections collected/unique	5906/1029
Data/restraints/parameters	1029/0/42
Final R indices $[F_o^2 > 2\sigma(F_o^2)]^a$	$R_1 = 0.0274$, $wR_2 = 0.0715$
R indices $(F_o^2 > 0)$	$R_1 = 0.0311$, $wR_2 = 0.0746$
Largest diff. Peak and hole (e Å^3)	1.981 and -1.974

[a] $R_1 = [\sum ||F_o| - |F_c||]/\sum |F_o|$. $wR_2 = \{[\sum w(|F_o| - |F_c|)_2/[\sum w(F_o^2)_2]]\}_{1/2}$. $w = \sigma_{F^2}$.

TABLE 2
Atomic Coordinates ($\times 10^4$) and Equivalent Isotropic Displacement Parameters ($Å^2 \times 10^4$) for $Yb_5In_2Sb_6$

Atom	x	y	z	U(eq)
Yb(1)	9584(1)	895(1)	5000	14(1)
Yb(2)	269(1)	2446(1)	5000	13(1)
Yb(3)	5000	0	5000	13(1)
Sb(1)	5465(1)	1369(1)	5000	12(1)
Sb(2)	54(1)	1897(1)	0	12(1)
Sb(3)	1989(1)	9992(1)	0	13(1)
In(1)	3244(1)	1202(1)	0	14(1)

Note. U(eq) is defined as one-third of the trace of the orthogonalized U_{ij} tensor.

RESULTS AND DISCUSSION

Structure. $Yb_5In_2Sb_6$ crystallizes in the $Ba_5Al_2Bi_6$ structure type (14). $Yb_5In_2Sb_6$ is anisotropic with one-dimensional character imparted by the presence of infinite $[In_2Sb_6]$ double chains. The double chains form from the condensation of single chains of $InSb_4$ tetrahedra bridged by Sb_2 dumbbell groups (Fig. 1). The projection along the c axis shows that the double $\frac{1}{\infty}[In_2Sb_6^{10-}]$ chains are arranged in parallel fashion so that they all lie on the ac plane. The next layer of double chains, below the ac plane, is crystallographically equivalent and related by b-glide and a-glide symmetry, respectively. Situated between the rows of $\frac{1}{\infty}[In_2Sb_6^{10-}]$, the Yb atoms provide charge balance and effective Coulomb screening. Curiously, the similar compound $Ba_5In_2Sb_6$ adopts the $Ca_5Ga_2As_6$-type structure in which the packing of the double chains is different, forcing a different arrangement of Ba atoms (Fig. 2) (15). Since all $Ba_5In_2Sb_6$, $Sr_5In_2Sb_6$, and $Ca_5In_2Sb_6$ are isostructural the larger size of Ba atoms than that of Yb atoms cannot explain the difference in structure types. Because of the similar sizes of Yb^{2+} and Ca^{2+}, $Yb_5In_2Sb_6$ is also expected to adopt the same structure. That it does not suggests that there are other factors operating besides the cation size that determine the overall structure. One such factor could be the more covalent bonding between the Yb^{2+} and Sb atoms in the structure (see below).

There are a large number of ternary compounds built by MPn_4 (M = Al, Ga; Pn = As, Sb). Such MPn_4 tetrahedral units have been found in the structures of $Ca_{11}InSb_9$, $Ca_{11}GaAs_9$, and $Ca_{14}AlSb_{11}$ (16), where the MPn_4 tetrahedra are isolated. However, in A_3MPn_3-type compounds (A = alkaline earth metals) such as Ba_3AlSb_3 and Ca_3AlSb_3, the tetrahedra are condensed to form oligomeric or polymeric entities. In Ba_3AlSb_3(17), two $AlSb_4$

TABLE 3
Anisotropic Displacement Parameters ($Å^2 \times 10^3$) for $Yb_5In_2Sb_6$

Atom	U_{11}	U_{22}	U_{13}	U_{33}	U_{23}	U_{12}
Yb(1)	15(1)	13(1)	15(1)	0	0	−2(1)
Yb(2)	10(1)	12(1)	16(1)	0	0	0(1)
Yb(3)	11(1)	12(1)	16(1)	0	0	−1(1)
Sb(1)	11(1)	10(1)	15(1)	0	0	0(1)
Sb(2)	11(1)	14(1)	11(1)	0	0	2(1)
Sb(3)	11(1)	15(1)	13(1)	0	0	−2(1)
In(1)	12(1)	16(1)	14(1)	0	0	1(1)

Note. The anisotropic displacement factor exponent takes the form $-2^2[h^2\,a^{*2}\,U_{11} + \cdots + 2h\,k\,a^*\,b^*\,U_{12}]$.

TABLE 4
Selected Bond Distances (Å) and Angles (°) in $Yb_5In_2Sb_6$

Sb(1)–In(1) × 2	2.8182(9)	Yb(3)–Sb(1) × 2	3.1682(11)
Sb(2)–In(1)	2.8504(12)	Yb(3)–Sb(3) × 4	3.1714(8)
Sb(3)–In(1)	2.9341(13)	Yb(1)–Yb(3)	3.9672(9)
Sb(3)–Sb(3)	2.9437(18)	Yb(1)–Yb(2)	4.0665(11)
In(1)–Sb(1) × 2	2.8183(9)	Yb(1)–Yb(1)	4.1611(14)
Yb(3)–In(1) × 4	3.7983(9)	Yb(2)–Yb(2) × 2	3.7080(9)
Yb(1)–Sb(1)	3.2376(12)	Yb(2)–Yb(1)	4.0665(11)
Yb(1)–Sb(2) × 2	3.2450(9)	In(1)–Sb(1)–In(1)	106.42(4)
Yb(1)–Sb(3) × 2	3.2567(8)	In(1)–Sb(3)–Sb(3)	107.74(4)
Yb(1)–Sb(3) × 2	3.5456(9)	Sb(3)–Sb(3)–Yb(3)	134.617(14)
Yb(1)–In(1) × 2	3.5953(10)	Sb(1)–In(1)–Sb(1)	106.42(4)
Yb(2)–Sb(1)	3.1847(11)	Sb(1)–In(1)–Sb(2)	113.97(3)
Yb(2)–Sb(1)	3.2158(11)	Sb(1)–In(1)–Sb(3)	108.30(3)
Yb(2)–Sb(2) × 2	3.2308(8)	Sb(2)–In(1)–Sb(3)	105.66(4)
Yb(2)–Sb(2) × 2	3.2392(8)		
Yb(2)–In(1) × 2	3.6664(10)		

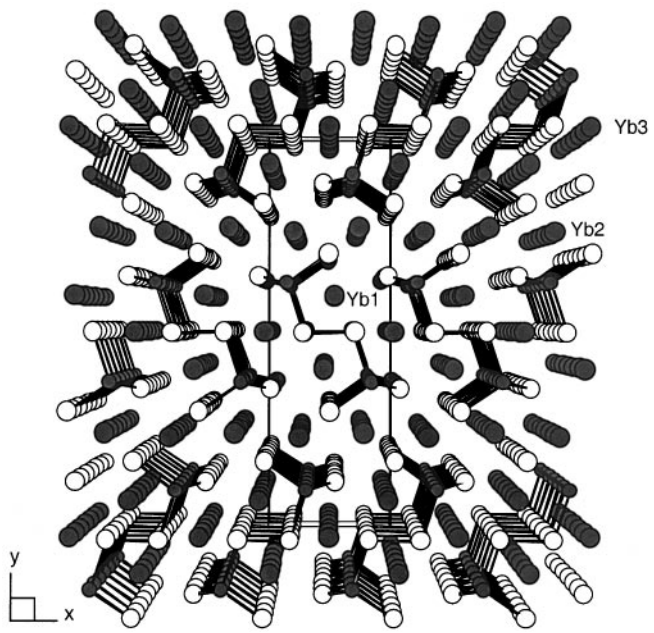

FIG. 1. A perspective view of the orthorhombic unit cell of $Yb_5In_2Sb_6$ down the [001] axis. The Yb atoms are labeled.

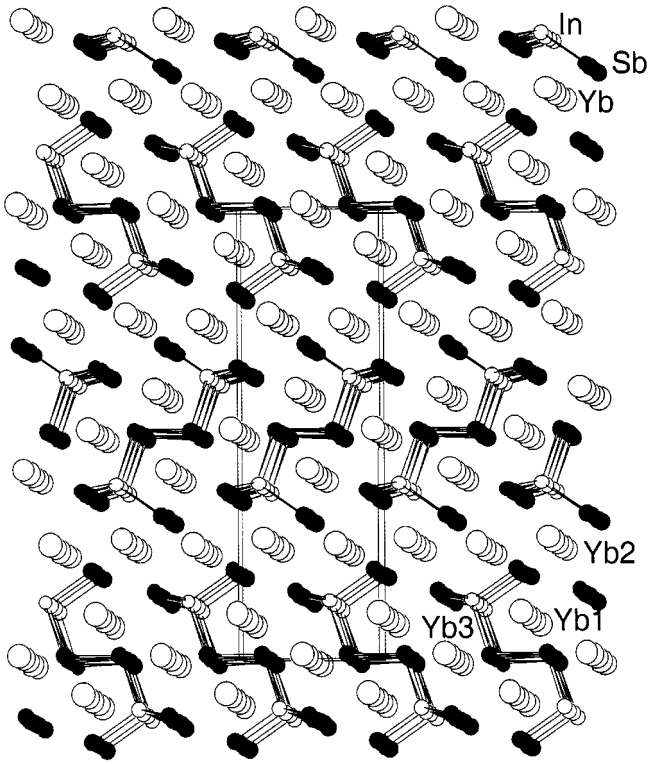

FIG. 2. A projection view of the orthorhombic unit cell of $Ba_5In_2Sb_6$ along the [001] axis.

tetrahedra share a common edge, forming a discrete dimeric anion $[Al_2Sb_6]^{12-}$, while with a smaller counterion as in Ca_3AlSb_3, a polymeric chain $\frac{1}{\infty}[AlSb_3^{6-}]$ made of two corner sharing tetrahedra is formed (18). In $Ca_5Al_2Sb_6$ (19), the $[Al_2Sb_6]^{12-}$ units are "oxidatively coupled" to double chains of the type observed in $Yb_5In_2Sb_6$. The coupling occurs via Sb_2 bridges to form $\frac{1}{\infty}[Al_2Sb_6^{10-}]$ double chains, as found in $Ca_5Ga_2As_6$-type compounds (19).

Figure 3 shows a fragment of a double chain with bond lengths and atomic labels. The Sb(3)–Sb(3) distance is 2.944 (2) Å, which is comparable to the Sb–Sb bond distances found in the zig-zag Sb chains of $Ba_4In_8Sb_{16}$ (3a) (2.949(2) Å). This is significantly longer than the Sb–Sb distances found in $Ca_5In_2Sb_6$, $Sr_5In_2Sb_6$, and $Ba_5In_2Sb_6$ (2.863–2.855(2) Å). Increasing the cationic size would require more space; however, the length of the Sb–Sb bond is not affected in this family of compounds. Instead, lengthening the In–Sb bonds and opening the angle of In–Sb–In fulfills the space requirement. The bond lengths in similar compounds are shown for comparison in Table 5. The origin of the Sb–Sb bond lengthening in $Yb_5In_2Sb_6$ is unclear, it is tempting to speculate a small degree of electron transfer from the Yb^{2+} ions to the σ^* antibonding orbital of the Sb–Sb unit.

TABLE 5
Bond Distances (Å) in $Ca_5Ga_2As_6$ and $Ca_5Al_2Bi_6$-Type Phases

Compounds	a^a	b^a	c^a	d^a	Structure type
$Ca_5In_2Sb_6$	2.810	2.826	2.954	2.863	$Ca_5Ga_2As_6$
$Sr_5In_2Sb_6$	2.840	2.836	3.025	2.855	$Ca_5Ga_2As_6$
$Ba_5In_2Sb_6$	2.892	2.853	3.100	2.855	$Ca_5Ga_2As_6$
$Ca_5Al_2Bi_6$	2.806	2.803	2.860	3.184	$Ca_5Al_2Bi_6$
$Yb_5In_2Sb_6$	2.818	2.850	2.934	2.944	$Ca_5Al_2Bi_6$

[a] See bond types for a, b, c, and d in Fig. 3.

There are three crystallographically unique Yb atoms in the structure. The local coordination environments of the Yb atoms are shown in Fig. 4. The Yb–Sb distances are in the range of 3.168–3.546 Å, which are comparable to the sum of covalent radii of Yb and Sb atoms (20). The Yb(2) and Yb(3) atoms are commonly in octahedra of Sb atoms. However, the Yb(1) atoms are in 7-coordination with capped trigonal prismatic geometry.

According to the Zintl concept, the formal charge of a four-bonded In atom can be assigned as In^{1-} and those of one- and two-bonded Sb atoms are assigned as Sb^{2-} and Sb^{1-} respectively. Therefore, the formula is best described as $(Yb^{2+})_5[2(In^{1-})4(Sb^{1-})2(Sb^{2-})]$. Alternatively, it can

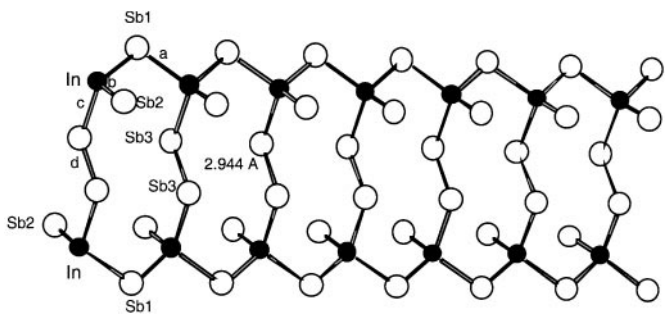

FIG. 3. Section of a $\frac{1}{\infty}[In_2Sb_6^{10-}]$ double chain with atomic labeling and bond lengths (Å). The double chains of tetrahedra and zigzag Sb chains are shown.

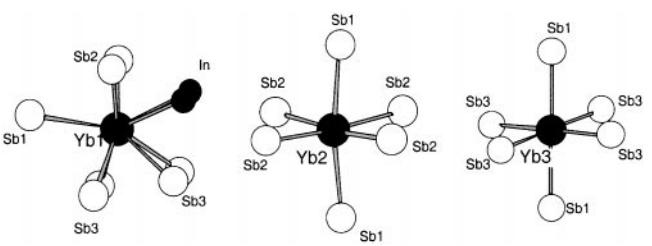

FIG. 4. Immediate coordination environment of the Yb atoms in $Yb_5In_2Sb_6$. In addition to the nearest Sb atoms around the Yb atoms, a few neighboring In atoms are also shown.

TABLE 6
Atomic Orbital Parameters[a] used in Extended Hückel Calculations

Atom	Orbital	H_{ii} (eV)[b]	$\zeta 1$[c]	C1	$\zeta 2$[d]	C2
Yb	6s	− 5.3500	1.5400	1.0000		
	6p	− 5.3500	1.5400	1.0000		
	5d	− 5.2100	2.8100	0.70634	1.2160	0.48343
	4f	− 13.860	8.629	0.74634	3.1980	0.45654
In	5s	− 12.600	1.90300	1.0000		
	5p	− 6.1900	1.67700	1.0000		
Sb	5s	− 18.7999	2.32300	1.0000		
	5p	−11.700000	1.99900	1.0000		

Note. [a] (a) M. Wolfsberg and L. Helmholz, *J. Chem. Phys.* **20,** 837 (1952); (b) C. J. Ballhausen and H. B. Gray, "Molecular Orbital Theory," Benjamin, New York, 1965.

[b] $H_{ii} = \langle \chi_i | H_{\text{eff}} | \chi_i \rangle$, $i = 1, 2, 3, \ldots$. The value approximated by valence–state ionization potential.

[c] Single zeta STOs.

[d] Double zeta STOs.

also be described as $(Yb^{2+})_5[(In^{3+})_2(Sb_2^{4-})(Sb^{3-})_4]$ using formal oxidation numbers.

Electronic structure. To understand the chemical bonding in this material and the role of the Yb states, band structure calculations were performed on $Yb_5In_2Sb_6$ and also on the anionic framework $[In_2Sb_6]^{10-}$. The band structures were calculated using the extended Hückel formalism with atomic orbital parameters given in Table 6. For comparison, the DOS plots of $Yb_5In_2Sb_6$ and $[In_2Sb_6]^{10-}$ around the Fermi level were drawn with a similar scale (Fig. 5). In DOS plots, the overall features of the valence band of $Yb_5In_2Sb_6$ and $(In_2Sb_6)^{10-}$ were similar except for a huge spike, in the former, well below the Fermi level. The spike at about − 14 eV is mainly due to the filled *f* states of the Yb atom. Usually, the *f* states of rare earth elements are well shielded by valence electrons; therefore, they do not play an important role in the chemical or transport properties. The valence bands near the Fermi level of $[In_2Sb_6]^{10-}$ and $Yb_5In_2Sb_6$ arise primarily from In *p* and Sb *p* orbitals mixed with corresponding *s* orbitals for sp^3 hybridization.

In the DOS plot of $[In_2Sb_6]^{10-}$ there is a peak just below the Fermi level that is mainly from p_z orbitals of Sb(3) with nonbonding character. However, in the DOS of $Yb_5In_2Sb_6$, the p_z states of Sb(3) in the valence band are moved down in energy, indicating significant mixing interactions between the Yb and Sb(3) states. In the conduction band of $Yb_5In_2Sb_6$, the Yb *s* and *p* states are well above the Fermi level as found in typical electron donors. The main effect of including Yb states in the calculation is to push the bottom of the conduction band down relative to the top of the valence band, effectively narrowing the band gap. The bottom of the broad conduction band mainly consists of p_x states of Sb(3). Even though we cannot estimate the exact quantitative change in the band gap, these results demonstrate that the band gap and band structure near the Fermi level can be modified significantly by the rare earth cations. Especially, narrow band gap semiconductors can be obtained with rare earth element analoges of alkaline earth Zintl compounds. Of course there is always the possibility of stabilizing new structures in rare earth containing Zintl phases due to strong orbital interaction between rare earth cations and anionic elements.

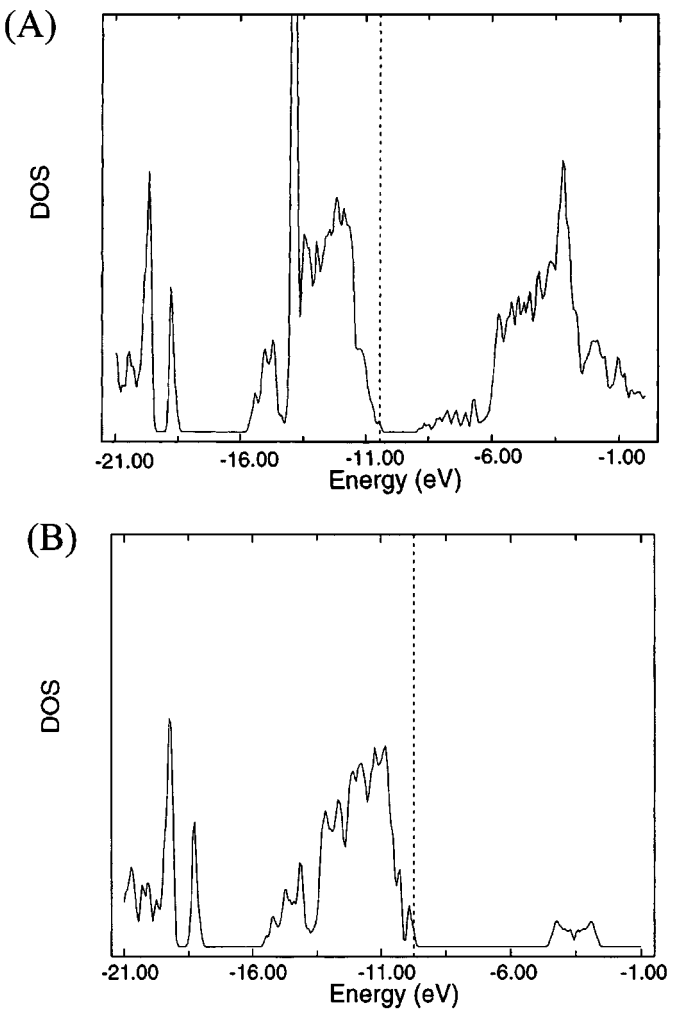

FIG. 5. (a) DOS curves of $Yb_5In_2Sb_6$. (b) DOS curves of $[In_2Sb_6]^{10-}$. The Fermi levels are indicated by dotted line.

Thermal and spectroscopic analysis. $Yb_5In_2Sb_6$ is stable in air at room temperature; however, when heated above 800°C, it slowly decomposes to InSb and an unknown amorphous Yb-rich Sb binary. The compound melts congruently at 767°C. A band gap was observed in the form of a broad absorption in the mid-IR region in the range of 0.2–0.4 eV, confirming the narrow gap nature of this

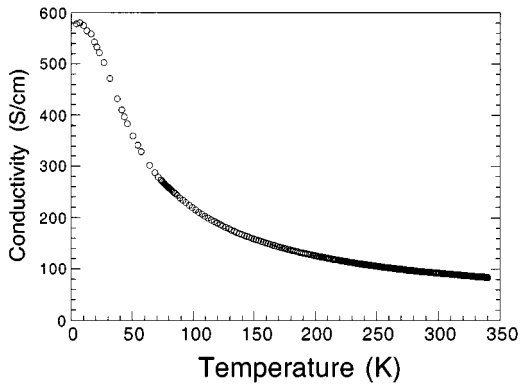

FIG. 6. Temperature dependence of the electrical conductivity for a polycrystalline ingot of $Yb_5In_2Sb_6$.

semiconductor. Because of a well-known drawback in the Hückel method the quantitative comparison of the calculated and experimental band gaps is not possible.

Charge and thermal transport measurements. The electrical conductivity and thermoelectric power of a polycrystalline ingot of $Yb_5In_2Sb_6$ were measured as a function of temperature. The conductivity at room temperature is ~ 100 S/cm, and it increases with falling temperature (see Fig. 6). This apparent metallic dependence is common in narrow gap semiconductors (21) and is attributed to doping impurities.

The value of thermoelectric power S (Seebeck coefficient) for $Yb_5In_2Sb_6$ was about $+30\ \mu V/K$ at room temperature and decreases almost linearly with decreasing temperature. The positive value of thermoelectric power indicates that $Yb_5In_2Sb_6$ is a *p*-type (hole) semiconductor. On the basis of the calculated band structure discussed above, the holes in this material reside primarily in the Sb sublattice. Efforts to fully characterize the thermoelectric properties in similar Zintl phases are now under way.

The room temperature thermal conductivity of this compound was measured at ~ 1.7 W/mK which is rather low. It is somewhat higher than optimized $Bi_{2-x}Sb_xTe_3$ alloys (1.5 W/mK) and closer to the value for pure Bi_2Te_3 at 1.8 W/mK. Given the rather low electrical conductivity of the electrical compound we expect the electronic contribution to the thermal conductivity to be negligible. Therefore, the measured value of 1.7 W/mK represents mainly the lattice thermal conductivity. The low value is attributed to three major factors, the presence of heavy rare earth atoms in the structure, the relatively low crystal symmetry, and the relatively large unit cell of the compound.

ACKNOWLEDGMENTS

Financial support from DARPA through the Army Research Office (DAAG55-97-1-0184) and the Department of Energy (Grant DE-FGO2-99ER45793) is gratefully acknowledged. S.-J. Kim acknowledges financial support from the Korean Science and Engineering Foundation (96-0501-0601-3).

REFERENCES

1. (a) T. M. Tritt, *Science* **283,** 804 (1999); (b) G. Mahan, B. Sale, and J. Sharp, *Physics Today* Jan., 42 (1997); (c) B. C. Sales, *MRS Bull.* Jan., 15 (1998); (c) D. M. Rowe, (Ed.), "CRC Handbook of Thermoelectrics," CRC Press, Boca Raton, FL, 1995; (d) M. G. Kanatzidis, and F. J. DiSalvo, *Thermoelectric Mater. Solid State Synth. ONR Q. Rev.* **27,** 14 (1996).
2. M. G. Kanatzidis, *Semimet. Semicond.* (2000), in press.
3. (a) S.-J. Kim, S. Hu, C. Uher, and M. G. Kanatzidis, *Chem. Mater.* **11,** 3154 (1999); (b) S.-J. Kim, and M. G. Kanatzidis, in preparation; (c) S.-J. Kim, S. Hu, C. Uher, T. Hogan, B. Huang, J. D. Corbett, and M. G. Kanatzidis, *J. Solid State Chem.* **153,** 321 (2000).
4. (a) S. M. Kauzlarich (Ed.), "Structure and Bonding of Zintl Phases and Ions." VCH, New York, 1996; (b) H. Schafer and B. Eisenmann, *Rev. Inorg. Chem.* **3,** 29,101 (1981).
5. (a) D.-Y. Chung, S. Jobic, T. Hogan, C. R. Kannewurf, R. Brec, J. Rouxel, and M. G. Kanatzidis, *J. Am. Chem. Soc.* **119,** 2505 (1997); (b) M. G. Kanatzidis, T. J. McCarthy, T. A. Tanzer, L.-H. Chen, L. Iordanidis, T. Hogan, C. R. Kannewurf, C. Uher, and B. Chen, *Chem. Mater.* **8,** 1465 (1996); (c) B. Chen, C. Uher, L. Iordanidis, and M. G. Kanatzidis, *Chem. Mater.* **9,** 1655 (1997); (d) D.-Y. Chung, K.-Y. Choi, L. Iordanidis, J. L. Schindler, P. W. Brazis, C. R. Kannewurf, B. Chen, S. Hu, C. Uher, and M. G. Kanatzidis, *Chem. Mater.* **9,** 3060 (1997); (e) L. Iordanidis, J. L. Schindler, C. R. Kannewurf, M. G. Kanatzidis, *J. Solid State Chem.* **143,** 151 (1999); (f) M. G. Kanatzidis, H. B. Lyon, G. D. Mahan, and T. M. Tritt (Eds.), "Thermolectric Materials—The Next Generation Materials for Small-Scale Refrigeration and Powder Generation Applications," *Mat. Res. Soc. Symp. Proc.* 545 (1999), and references therein.
6. J. Y. Chan, M. M. Olmstead, S. M. Kauzlarich, and D. Webb, *J. Chem. Mater.* **10,** 3583 (1998).
7. (a) R. B. Coles, *Contemp. Phys.* **28,** 143 (1994); (b) F. Steglich, C. Geibel, K. Gloss, G. Olesch, C. Schank, C. Wassilew, A. Loidl, A. Krimmel, and R. G. Stewart, *J. Low Temp. Phys.* **95,** 3 (1994); (c) M. B. Maple, *Physica B* **171,** 389 (1991).
8. H. O. Marcy, T. J. Marks, and C. R. Kannewurf, *IEEE Trans. Instrum. Meas.* **39,** 756 (1990).
9. (a) R. Hoffman, *J. Chem. Phys.* **39,** 1397 (1963); (b) E. Canadell and M.-H. Whangbo, *Chem. Rev.* **91,** 965 (1991).
10. J. Ren, W. Liang, and M.-H. Whangbo, CAESAR 1.0 Primecolor Software, Inc., Cary, NC, 1998.
11. SMART: Siemens Analytical X-Ray Systems, Inc., Madison, WI, 1996.
12. SAINT, Version 4: Siemens Analytical X-Ray System, Inc., Madison, WI, 1994.
13. SHELXTL, Version 5; Siemens Analytical X-Ray System, Inc., Madison, WI, 1994. G. M. Sheldrick, University of Göttingen, Germany, to be published.
14. (a) G. Cordier, H. Schäfer, and M. Stelter, *Z. Naturforsch. B* **40,** 975 (1985); (b) G. Cordier, H. Schäfer, and M. Stelter, *Z. Naturforsch. B* **40,** 1100 (1985); (c) G. Cordier, H. Schäfer, and M. Stelter, *Z. Naturforsch. B* **39,** 727 (1984).
15. G. Cordier and M. Stelter, *Z. Naturforsch.* **43,** 453 (1987).
16. (a) G. Cordier, H. Schäfer, and M. Stelter, *Z. Naturforsch. B* **40,** 868 (1985); (b) S. L. Brock, L. J. Weston, M. M. Olmsted, and S. M. Kauzlarich, *J. Solid State Chem.* **107,** 513 (1993); (c) G. Cordier and G. Schäfer, *Z. Anorg, Allg. Chem.* **519,** 183 (1984).
17. (a) G. Cordier, G. Savelsberg, and H. Schäfer, *Z. Naturforsch. B* **37,** 975 (1982); (b) G. Cordier, H. Schäfer, and M. Stelter, *Z. Naturforsch. B* **40,** 1100 (1985).

18. G. Cordier, H. Schäfer, and M. Stelter, *Z. Naturforsch. B* **39,** 727 (1984).
19. (a) G. Cordier, H. Schäfer, and M. Stelter, *Z. Naturforsch. B* **40,** 5 (1985); (b) G. Cordier and M. Stelter, *Z. Naturforsch. B* **43,** 463 (1988); (c) P. P. Verdier, P. L'Haridon, M. Maunaye, and Y. Laurent, *Acta. Crystallogr. Sect. B* **32,** 726 (1976).
20. J. Donohue, "The Structure of the Elements." Wiley, New York, 1974.
21. (a) H.-H. Jeon, H.-P. Ha, D.-B. Hyun, and J.-D. Shim, *J. Phys. Chem. Solids* **4,** 579 (1991); (b) L. R. Testardi, J. N. Bierly, Jr., and F. J. Donahoe, *J. Phys. Chem. Solids* **23,** 1209 (1962).